Rewiring of RSK–PDZ Interactome by Linear Motif Phosphorylation

Gergő Gógl[1], Beáta Biri-Kovács[1], Fabien Durbesson[2], Pau Jane[3], Yves Nomine[3], Camille Kostmann[3], Viktória Bilics[1], Márton Simon[1], Attila Reményi[4], Renaud Vincentelli[2], Gilles Trave[3] and László Nyitray[1]

1 - Department of Biochemistry, ELTE Eötvös Loránd University, Budapest, Hungary
2 - Unite Mixte de Recherche (UMR) 7257, Centre National de la Recherche Scientifique (CNRS) Aix-Marseille Universite, Architecture et Fonction des Macromolécules Biologiques (AFMB), Marseille, France
3 - Equipe Labellisee Ligue 2015, Department of Integrated Structural Biology, Institut de Genetique et de Biologie Moleculaire et Cellulaire (IGBMC), INSERM U1258/CNRS UMR 7104/Universite de Strasbourg, 1 rue Laurent Fries, BP 10142, F-67404 Illkirch, France
4 - Institute of Enzymology, Research Center for Natural Sciences, Hungarian Academy of Sciences, Budapest, Hungary

Correspondence to Gilles Trave and László Nyitray: trave@esbs.u-strasbg.fr, nyitray@elte.hu
https://doi.org/10.1016/j.jmb.2019.01.038
Edited by Mingjie Zhang

Abstract

Phosphorylation of short linear peptide motifs is a widespread process for the dynamic regulation of protein–protein interactions. However, the global impact of phosphorylation events on the protein–protein interactome is rarely addressed. The disordered C-terminal tail of ribosomal S6 kinase 1 (RSK1) binds to PDZ domain-containing scaffold proteins, and it harbors a phosphorylatable PDZ-binding motif (PBM) responsive to epidermal growth factor stimulation. Here, we examined binding of two versions of the RSK1 PBM, either phosphorylated or unphosphorylated at position −3, to almost all (95%) of the 266 PDZ domains of the human proteome. PBM phosphorylation dramatically altered the PDZ domain-binding landscape of RSK1, by strengthening or weakening numerous interactions to various degrees. The RSK–PDZome interactome analyzed in this study reveals how linear motif-based phospho-switches convey stimulus-dependent changes in the context of related network components.

Background

Protein–protein interactions form a functional network, the interactome, which can be dynamically regulated by the phosphorylation of network components on disordered protein regions [1]. These so-called linear motifs most often bind to structured domains, such as (PSD95/DLG1/ZO-1) PDZ domains. PDZ domains belong to one of the most common families of globular domains, with 266 members in the human proteome [2]. They recognize short linear motifs called PDZ-binding motifs (PBMs) at the extreme C-terminus of their target proteins (canonical PBMs) or within internal regions (non-canonical PBMs). Canonical PBMs systematically contain a hydrophobic residue (most frequently Val or Leu) at their C-terminus (numbered as position 0) and are classified in three main classes based on the residue at minus 2 position (Ser/Thr in the most common class 1, hydrophobic in class 2 and acidic in class 3) [3]. In principle, the general consensus sequence determining a PBM allows for the presence of potentially phosphorylatable residues at any positions except the hydrophobic C-terminal position [4].

PDZ–PBM interactions are involved in various cellular processes and are especially common in intracellular signaling pathways. For example, all isoforms of the ribosomal S6 kinase (RSK) of the MAPK pathway contain a functional class 1 PBM [5]. RSK has an emerging role in multiple cancer types such as glioblastoma or melanoma [6,7]. Upon mitogenic stimulation, a series of phosphorylation events leads to the activation of the MAP kinase ERK1/2 [8]. RSK is one of the strongest interaction partners of ERK (compared to other docking motif facilitated MAPK interactions), and its complex activation mechanism is

also initiated by ERK phosphorylation (Fig. 1A) [9–11]. The C-terminal tail of RSK is a multifunctional linear motif as it contains partially overlapping binding sites for ERK, S100B, a tyrosine kinase, phosphatase(s), and PDZ domains [12–14]. In addition, activated RSK will autophosphorylate its own PBM within its intrinsically disordered tail, which will probably affect all of these interactions [15]. The RSK1 PBM contains three potential autophosphorylation sites, while other isoforms contain only two (Fig. 1B). Among these, Ser732 is found at the minus 3 position [16,17]. Thomas *et al.* [5] observed no change with RSK1/2 phosphomimics (at −3) in their interaction with MAGI1, SHANK1 or GRIP1, and they suggested that both inactive and active RSKs likely bind to PDZ domain proteins. Similarly, our recent work showed that phosphorylation of RSK1 only mildly changed the interaction with MAGI1 [15]. In contrast, a recent publication revealed that the phosphorylation (or a phosphomimetic mutation) at the analogous site triggered the association between RSK1/3 and the PDZ domain of SCRIBBLE and abolished the interaction between RSK3 and the PDZ domain of SHANK1 [18]. These results indicated that RSK activation might induce a complex reshuffling of its PDZ domain mediated interactome.

In order to elucidate the impact of phosphorylation of a given PBM, binding to all of its putative partners in the human proteome needs to be measured, quantitatively. In addition, *in vitro* observed changes need to be validated in cell-based assays. To address these challenges, we applied here a recently developed high-throughput approach [19] to measure the individual binding affinities of the 266 known human PDZ domains for both the unphosphorylated and phos-

phorylated RSK1 PBMs. Furthermore, we used luciferase complementation assay to measure the effect of epidermal growth factor (EGF) stimulation on full-length RSK–PDZ interactions in HEK293T cells. Our work reveals new kinase-scaffold complexes, the mechanism of PDZ domain-based RSK substrate targeting, and identifies new functions of RSK1.

Results

PDZome-binding profiles of native and phosphorylated RSK1 PBMs

To investigate how phosphorylation can modulate the binding of the RSK1 PBM to PDZ domains, we used the automated high-throughput holdup assay, which allows to measure binding intensities (BIs) for a large number of domain-motif pairs. As compared to the original work describing this approach [19], we used an updated version of our PDZ library, including all the 266 known human PDZ domains [20]. We were able to quantify the interaction of 255 PDZ for the unphosphorylated RSK1 peptide and 252 for the phosphorylated form (96% and 95% of the human PDZome, respectively). Both data sets were plotted in the form of "PDZome-binding profiles" (Fig. 2A) representing all the individual BIs measured for each PDZ domain for the unphosphorylated and phosphorylated RSK peptides, respectively. Using BI = 0.2 as the minimal threshold for a significant PDZ–peptide interaction, the holdup assay identified 34 potential RSK1 binders, including 26 PDZ binders for the unphosphorylated peptide and 25 binders for the phospho-peptide (Figs. 2A and S1,
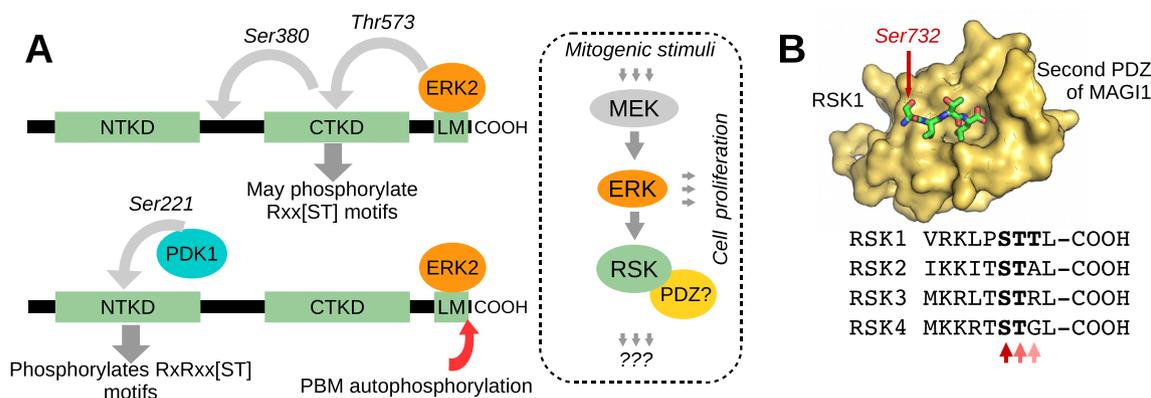

Fig. 1. The activation of RSK includes a feedback phosphorylation site that can affect PDZ binding. (A) Activation of the tandem kinase RSK is a multi-step process. Activation of RSK is initiated by ERK docking, which is followed by the phosphorylation of the C-terminal kinase domain (CTKD) [9]. The active CTKD phosphorylates a linker site between the kinase domains that creates a docking site for PDK1 [11]. In the end, PDK1 activates the N-terminal kinase domain (NTKD) [10]. Usually, only the NTKD is considered as an effector kinase, and the CTKD is only associated with a self-regulatory role, but one of these activated kinases phosphorylates its C-terminal PBM. While RSK is an effector of the mitogenic ERK pathway, its downstream effects are not well explored. (B) Each RSK isoforms contain a functional class 1 PBM. RSK1 contains 3 mutually exclusive autophosphorylation sites (at the minus 1, 2, and 3 positions) and the other isoforms contain only two (at the minus 2, 3 positions), but only the minus 3 site (Ser732 in RSK1) is considered as a major feedback site [16]. The structural panel shows RSK1 binding to the second PDZ domain of MAGI1.
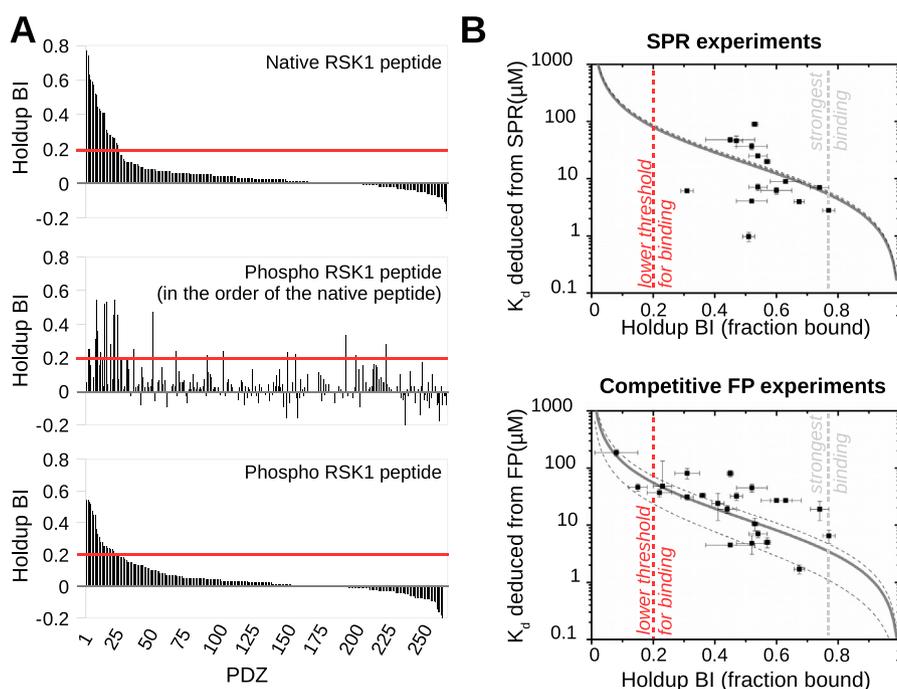
Fig. 2. PDZome binding of RSK1 explored by *in vitro* protein–peptide binding assays. (A) PDZome-binding profiles of unphosphorylated and phosphorylated RSK1 PBMs. A red line indicates the cutoff for a significant PDZ–PBM interaction (BI > 0.2). PDZ domains in the upper and lower plots are ranked on the basis of their BIs for the indicated peptide. In the middle plot, PDZ domains are ranked on the basis of their BIs for the unphosphorylated peptide, while the plotted BI values are those obtained for the phosphopeptide. Note the considerable reshuffling of binding ligands induced by phosphorylation. (B) Comparison of orthogonal binding data obtained by the holdup assay, SPR, and an FP-based assay. The correlation of BIs obtained by holdup assays to the affinities deduced from SPR or competitive FP measurements was fitted using a Monte Carlo approach. Despite the independent affinity measurement procedures, a similar correlation was observed in both cases. The fitting procedure delivers a value for the peptide concentration in the holdup assay, combining this with the free and peptide-bound PDZ domain concentrations (both delivered by the holdup assay); the dissociation constant of all human PDZ domains could be determined.

Table S1). The general distribution of the PDZome-binding profiles was similar in both cases. However, phosphorylation decreased the maximal and average BIs from 0.77 to 0.54, and from 0.42 to 0.33, respectively. Furthermore, the order of the PDZ domains that bind best to the unphosphorylated and phosphorylated RSK1 PBM was markedly different, as visually illustrated by the global reshuffling of their respective profiles (Fig. 2A). Using the same threshold for significant binding, the phosphorylated RSK1 PBM lost 12 of the detectable binders and gained 10 new binders as compared to the unphosphorylated peptide. This implies that at least 35% of the potential binders interact (often with variable affinities) to both phosphorylated and native RSK1 peptides, while the rest of them bind detectably to only one state of the RSK1 PBM.

In vitro validation of PDZ–RSK interactions by biophysical approaches

To validate the results of the holdup assay, we used orthogonal *in vitro* approaches: isothermal titration calorimetry (ITC), surface plasmon resonance (SPR-

Biacore), direct and competitive fluorescence polarization (FP) (Table 1, Figs. S2 and S3). To benchmark the BIs of the holdup assay against steady-state dissociation constants, we decided to systematically test by high-throughput techniques (SPR-Biacore and competitive FP) those interactions that showed a BI value larger than 0.4 in any of the two holdup assays (Table 1, and Figs. S2 and S3). With these methods, we were able to accurately measure binding constants of 15 and 28 PDZ–PBM pairs, respectively. These experiments quantitatively confirmed the phosphorylation-induced changes in binding affinities, which were originally detected by the holdup assay. For example, a 3- to 6-μM dissociation constant was apparent between the PDZ of ARHGEF12 and the native RSK1 peptide, while no interaction could be detected with the phosphorylated state. Vica versa, the PDZ domain of SYNJ2BP interacted with the phosphorylated peptide with a 10- to 20-μM dissociation constant, while no interaction was detectable with the native state.

We used these data sets to estimate the quantitative correlation between measured BIs and the dissociation constants using Monte Carlo modeling and a general

Table 1. Summary of the *in vitro* experiments

	BI	K_D, direct FP (µM)	K_D, competitive FP (µM)	K_D, SPR (µM)	K_D, SPR, HPV16 E6 (µM)	K_D, estimated (µM)	Fold change
ARHGEF12	0.77 ± 0.02; 0.05 ± 0.05	7.5 ± 0.8; 29 ± 8	6.6 ± 1.7; >100	2.79 ± 0.11; no binding	10.9 ± 1.4	4.2; >100	0.04
GRID2IP-2	0.67 ± 0.02; 0.00 ± 0.01	5.1 ± 0.4; 47 ± 15	1.7 ± 0.3; 85 ± 11	3.96 ± 0.12; no binding	No binding	7.1; >100	0.07
MAST2	0.74 ± 0.03; 0.23 ± 0.03	7.9 ± 0.6; 13 ± 2	19 ± 7; 48 ± 84	7.02 ± 0.27; no binding	2.5 ± 0.2	4.9; 53.8	0.09
PDZD7–3	0.60 ± 0.03; 0.15 ± 0.03	0.80 ± 0.05; 1.8 ± 0.1	4 ± 1; 46 ± 7	6.2 ± 0.9; no binding	No binding	9.7; 92.9	0.10
MAST1	0.57 ± 0.01; 0.08 ± 0.03	26 ± 4; 34 ± 8	5 ± 1; 92 ± 12	20 ± 1; no binding	No binding	11.1; >100	0.11
GOPC	0.63 ± 0.05; 0.25 ± 0.10	20 ± 1; >100	27 ± 2; >100	8.92 ± 0.44; no binding	No binding	8.5; 48.0	0.18
MAGI1–2	0.43 ± 0.02; 0.15 ± 0.02	ND; ND	ND; ND	No binding, no binding	3.4 ± 0.8	20.3; 92.9	0.22
NHERF3–1	0.41 ± 0.01; 0.03 ± 0.01	80 ± 20; 220 ± 30	ND; ND	No binding, no binding	23 ± 3	22.1; >100	0.22
GORASP2	0.41 ± 0.02; 0.19 ± 0.01	67 ± 33; 114 ± 35	ND; ND	No binding, no binding	No binding	22.1; 69.2	0.32
GRASP	0.29 ± 0.01; 0.04 ± 0.01	ND; ND	ND; ND	ND; ND	ND	38.8; >100	0.38
PARD3B-1	0.52 ± 0.05; 0.31 ± 0.02	27 ± 3; 6.8 ± 0.5	45 ± 7; 31 ± 3.5	4.0 ± 0.3; 6.1 ± 0.4	No binding	13.8; 35.1	0.39
MAGI2–2	0.42 ± 0.01; 0.23 ± 0.03	420 ± 30; 430 ± 45	ND; ND	No binding, no binding	2.9 ± 0.14	21.2; 53.8	0.39
ARHGEF11	0.28 ± 0.06; 0.01 ± 0.02	ND; ND	ND; ND	ND; ND	ND	40.8; >100	0.40
SHANK3	0.27 ± 0.03; 0.07 ± 0.01	ND; ND	ND; ND	ND; ND	ND	43.0; >100	0.43
DFNB31–3	0.23 ± 0.04; −0.01 ± 0.02	ND; ND	ND; ND	ND; ND	ND	53.8; >100	0.53
NHERF2–2	0.20 ± 0.04; 0.07 ± 0.05	ND; ND	ND; ND	ND; ND	ND	64.8; >100	0.64
HTRA1	0.44 ± 0.03; 0.36 ± 0.01	30 ± 2; 11.3 ± 0.4	19 ± 3; 33 ± 2	No binding, no binding	No binding	19.4; 27.7	0.70
MAGI3–2	0.28 ± 0.03; 0.28 ± 0.06	ND; ND	ND; ND	ND; ND	ND	40.8; 40.8	1.00
PDZRN4–1	0.51 ± 0.02; 0.54 ± 0.03	33 ± 5; 14 ± 2	ND; ND	0.97 ± 0.18; 7.1 ± 0.9	6.0 ± 1.5	14.4; 12.6	1.14
SNTG2	0.41 ± 0.02; 0.52 ± 0.05	65 ± 2; 24 ± 2	24 ± 12; 4.8 ± 1.7	No binding; 37 ± 5	No binding	22.1; 13.8	1.60
PTPN3	0.05 ± 0.02; 0.21 ± 0.02	ND; ND	ND; ND	ND; ND	ND	>100; 60.8	1.66
SHROOM2	0.00 ± 0.01; 0.21 ± 0.01	ND; ND	ND; ND	ND; ND	ND	>100; 60.8	1.66
LIMK2	0.01 ± 0.06; 0.22 ± 0.07	ND; ND	ND; ND	ND; ND	ND	>100; 57.2	1.77
GORASP1	0.01 ± 0.02; 0.23 ± 0.03	ND; ND	ND; ND	ND; ND	ND	>100; 53.8	1.88
GRID2IP-1	0.06 ± 0.02; 0.24 ± 0.01	ND; ND	ND; ND	ND; ND	ND	>100; 50.8	1.99
LNX1–3	0.04 ± 0.02; 0.24 ± 0.07	ND; ND	ND; ND	ND; ND	ND	>100; 50.8	1.99
DLG4–2	0.11 ± 0.03; 0.25 ± 0.02	ND; ND	ND; ND	ND; ND	ND	>100; 48.0	2.10
PDZRN3–1	0.26 ± 0.01; 0.45 ± 0.01	90 ± 25; 17.5 ± 1.4	>100; 80 ± 10	No binding, no binding	8.6 ± 1.6	45.4; 18.6	2.45
LAP2	−0.02 ± 0.05; 0.28 ± 0.01	ND; ND	ND; ND	ND; ND	ND	>100; 40.8	2.47
SNTA1	0.31 ± 0.04; 0.53 ± 0.01	41 ± 11; 4.9 ± 0.4	81 ± 17; 10.5 ± 2.6	No binding; 90 ± 4	101 ± 40	35.1; 13.2	2.66
SNTB1	0.22 ± 0.04; 0.45 ± 0.08	18 ± 2; 1.5 ± 0.1	37 ± 6; 4.5 ± 0.3	No binding; 48 ± 5	27 ± 4	57.2; 18.6	3.08
PPP1R9A	0.00 ± 0.02; 0.33 ± 0.02	ND; ND	ND; ND	ND; ND	ND	>100; 31.8	3.17
SYNJ2BP	0.26 ± 0.07; 0.54 ± 0.03	39 ± 2; 16 ± 1	>100; 7 ± 1	No binding; 25 ± 1	33 ± 4	45.4; 12.6	3.59
SNX27	0.08 ± 0.07; 0.47 ± 0.02	25 ± 6; 4.4 ± 0.4	185 ± 25; 32 ± 5	No binding; 46 ± 9	No binding	>100; 17.1	5.92

Values after the semicolon correspond to the phosphorylated RSK1 peptides. HPV16 E6 was used as an internal standard during the SPR measurements. K_d estimation was calculated from BI values as described in Materials and Methods and using an estimated 17 µM peptide concentration. Fold changes were calculated by dividing the estimated unphosphorylated and the phosphorylated dissociation constants. For undetectable interactions, a very weak K_d was assumed (100 µM, which corresponds to a BI of 0.14). ND means not determined, while no binding means that it was impossible to quantitatively measure their affinities in our experimental conditions.

equation of the dissociation constant. While different experimental methods resulted slightly different affinities (where only two K_d pairs showed larger than a magnitude difference), their independent fits resulted similar conclusions. We have found that the peptide concentration in the holdup assays was between 14 and 23 μM (Fig. 2B, Table 1). Using this fitted parameter, it can be calculated that the holdup assay was capable of detecting any interaction with $K_d < 65$ μM (at the 0.2 BI cutoff).

Dynamic rearrangement of the RSK1–PDZ interactome *in vitro*

The holdup assay identified ARHGEF12 as the strongest interaction partner of the unphosphorylated peptide (BI = 0.77; $K_D \approx 4$ μM) (Fig. 3 and Tables 1, S1). This protein is a RhoA GEF. It has recently been reported that its interaction with RSK2 is essential in RhoA activation and that this interaction leads to increased cell motility in the U87MG glioblastoma cell line [21]. We also identified strong interaction with MAST2, which is an AGC kinase similarly to RSK (BI = 0.74; $K_D \approx 5$ μM) [22]. The previously characterized interaction between MAGI1 and RSK1 was found among the top binders of the unphosphorylated data set (BI = 0.43; $K_D \approx 20$ μM). Interestingly, our approach shows that phosphorylation down-regulate this interaction by a factor of five in contrast to earlier works [5,15]. This is very likely due to the limited dynamic change of other methods (such as ITC) in

cases of very weak interactions (e.g., compare Fig. S3B with S3B or S2). The strongest interaction partners of the phosphorylated PBM were three signal transducing adaptor proteins SYNJ2BP, SNTA1, and the E3 ubiquitin ligase PDZRN4 (in all cases BI ≈ 0.54; $K_D \approx 13$ μM) (Fig. 3, Tables 1 and S1).

Approximately one third of the identified PDZ interaction partners of RSK1 were capable to interact with both states of the PBM (Fig. 3B). By using the holdup assay, we had the unique opportunity to gain quantitative insight into the dynamic changes that occur after a single phosphorylation event (Fig. 3C). At the two extremes, RSK1 was engaged in OFF and ON "phospho-switches" (according to our detection threshold) with ARHGEF12 and SNX27, respectively. All other interactions showed a gradual modulation by phosphorylation. In conclusion, we provided *in vitro* experimental evidence that phosphorylation reshuffles the whole RSK1–PDZ interactome.

The dynamics of RSK1–PDZ interactions in cells

The observed changes in steady-state binding affinities suggested large-scale rewiring of the RSK–PDZ interactions. To test this concept, we validated selected interactions in a cellular context using a split-luciferase fragment complementation system, called NanoBiT. This method is appropriate for detecting dynamic changes in PPIs [23]. Instead of using isolated, purified PDZ domains and RSK peptides, we used full-length proteins in HEK293T cells. Wild type
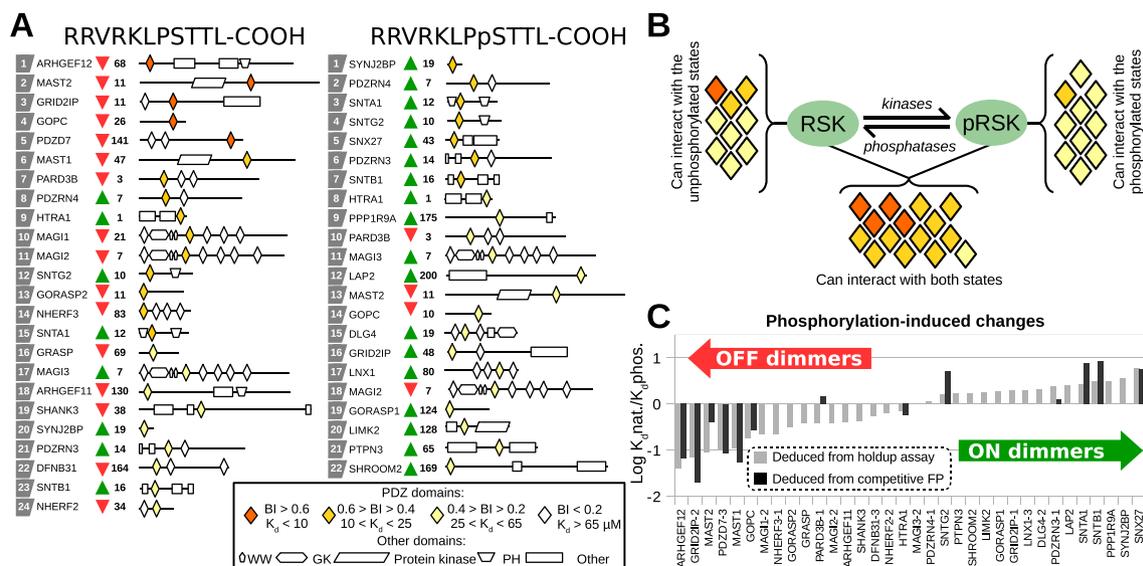

Fig. 3. Binding affinity changes elicited by PBM phosphorylation. (A) Domain architecture of the identified interaction partners. The PDZ domains are colored according to the measured BI values. (B) Using lowered cutoffs in the holdup assay ($K_d < 100$ μM), almost half of the identified RSK1 interaction partners showed detectable affinity to both states of the RSK1 C-terminal peptide. (C) Phosphorylation promotes a complex rearrangement in the RSK1 PDZ interactome. Instead of two definite classes (ON or OFF switching), a continuum (ON or OFF dimming) was measured in the phosphorylation-induced K_d differences of the holdup assay. Dark gray columns show the experimentally determined K_d differences from the competitive FP measurements.

(WT) and two mutant versions of RSK1 were used. The L714E mutation eliminates the interaction between ERK and RSK; therefore, RSK cannot be activated [9]. The ΔC1 truncation eliminates the last residue of RSK1 and thus suppresses the functional PBM of the protein [15]. We obtained high luminescence signals with the ARHGEF12, GOPC, PARD3B, MAGI1, and SYNJ2BP sensors in serum-starved cells (Fig. 4A). The C-terminal truncation significantly reduced the lumines-

cent signal in all cases, while the L714E mutation decreased the luminescence outputs for PARD3B and SYNJ2BP.

EGF stimulation can be used to turn on the ERK signaling cascade, RSK activation and its PBM autophosphorylation [24]. Extracellular stimulation induced changes in NanoBiT sensor brightness within the same timescale as ERK–RSK dissociation (Fig. 4B). In all cases, the maximum change was
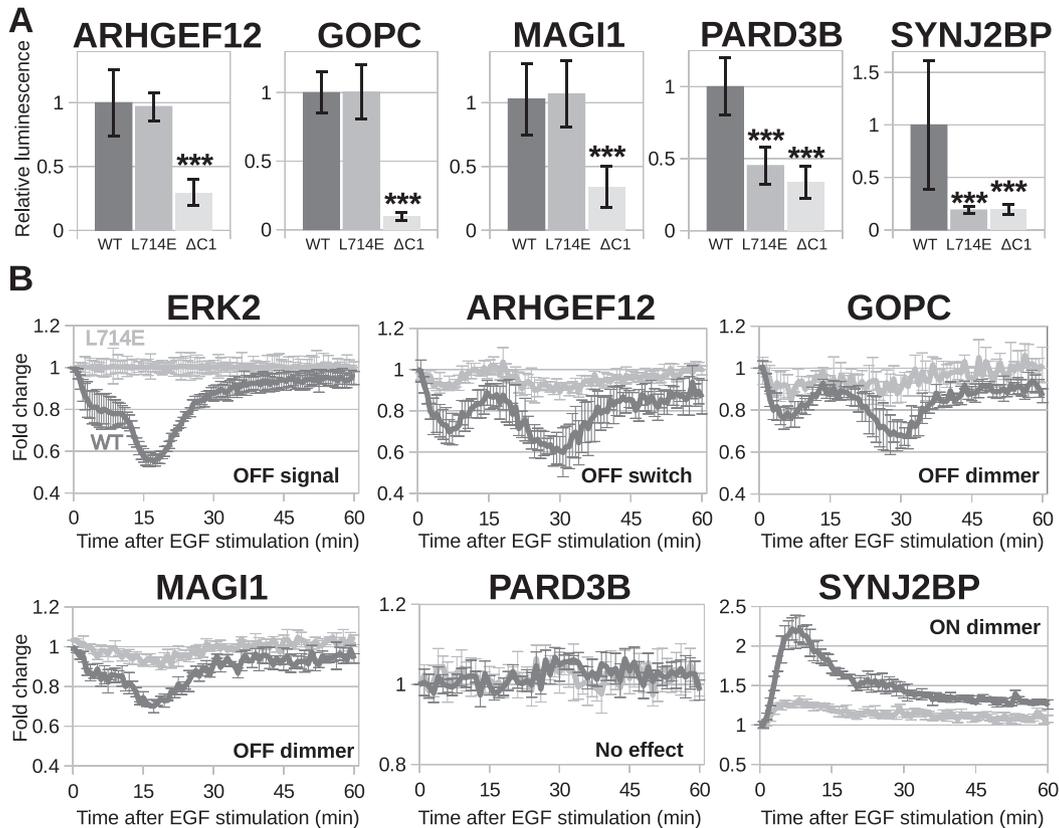

Fig. 4. Live-cell monitoring of RSK1 binding to PDZ-containing partners. (A) Monitoring steady-state luminescence with the interaction sensors between RSK1 and full-length PDZ proteins. Full-length proteins fused to two complementary fragments of nanoluc luciferase were co-expressed in serum starved HEK293T cells. The resulting luminescence signal was measured as indicated in the Materials and Methods. The luminescence signal obtained for the pair of WT constructs is used as reference (relative luminescence). The L714E RSK1 mutant is known to eliminate the interaction between RSK1 and ERK [9]. The ΔC1 RSK1 mutant does not contain the last C-terminal residue of RSK1 and therefore does not contain a functional PBM. The luminescence signal is consistently disrupted by the ΔC1 mutation, indicating that this signal reports on the PBM-mediated binding of RSK1 to its PDZ-containing targets. The L714E mutation disrupts the signal in cases where the interaction partner can significantly interact with the phosphorylated form of RSK1 (n = 6). Asterisks indicate statistical significance (***$P < 0.001$) calculated by two-tailed Student's *t* test between the luminescence signals of mutant and WT RSK1 constructs. (B) RSK1-based luminescence interaction sensors (with ERK2 and several proteins containing RSK1-binding PDZ domains) were co-expressed in serum-starved HEK293T cells. The luminescence signal in absence and in presence of EGF (20 ng/ml) was monitored for 60 min following EGF addition. The measured luminescence signal was normalized to the initial luminescence and to the spontaneous substrate (furimazine) decay based on the unstimulated cells. The dark and gray curves show the luminescence signals of the WT and the L714E mutant, respectively. EGF stimulation provokes a time-modulated decrease of the luminescence signal for co-expressed constructs of RSK1 and ERK2 as observed in our previous work [15]. Note that EGF stimulation diversely modulates the luminescence signal (increase, decrease, or no significant change) for each PDZ-containing protein in a comparable timescale to that of RSK-ERK dissociation. Remarkably, in this cell-based assay, using full-length proteins, EGF-induced luminescence signal modulation shows a good agreement to the results of *in vitro* measurements where only an RSK1 PBM peptide and PDZ domains constructs were used.

detectable between 10 and 20 min and the signal started to disappear after 30–45 min. As in our previous study [15], we observed periodic signals, which seem to be a characteristic feature of RSK-based interactions. ARHGEF12, GOPC, and MAGI1 showed a decrease in luminescence after stimulation. In contrast to these OFF signals, PARD3B did not show any change after activation of the pathway, while SYNJ2BP showed an increased luminescence after EGF stimulus. Results of this cell-based PPI tests showed a good agreement with *in vitro* measurements.

A compendium of potential RSK targets

Our high-throughput study identified a wealth of novel RSK-binding PDZ domains. The proteins that contain these RSK-binding PDZ domains represent in principle, candidate substrates of RSK kinases. In previous studies, only a few PDZ-containing partners of RSKs were assumed to be substrates [5,15,25]. To investigate this issue, we collected RSK-focused phosphoproteomic data sets for a meta-analysis. To our knowledge, there are three such data sets. (i) Galan *et al.* [26] searched for RSK substrates using specific inhibitors. (ii) Moritz *et al.* [27] tried to find tyrosine kinase activated AGC kinase substrates. (iii) Avey *et al.* [28] used the viral ORF45 protein to activate the ERK–RSK axis in cells, and they searched for up- or down-regulated phosphoproteins. (iv) In addition, a compendium of ERK targets has recently been published [29]. It is a systematic collection of ERK related phosphoproteomic studies containing both direct and indirect ERK substrates. The compendium is also a valuable resource for potential RSK phosphosites (Rxx[ST] and RxRxx[ST] motifs) [26]. The compendium contains 1477 [ST]P sites (from 892 proteins), 544 Rxx[ST] sites (from 430 proteins), and 458 other phosphorylation sites (from 330 proteins). We used this Rxx[ST] subset of the ERK compendium as an additional resource to our meta-analysis. The collection of four potential RSK substrates, termed here as RSK compendium, included 997 potential substrates, where 349 substrates were identified in more than one study (Fig. 5A, Table S2). Only 35 substrates were identified in all four phosphoproteomic data sets, including some well-characterized RSK substrates, such as ARHGEF12, EIF4B, EphA2, GSK3B, PFKFB2, PPP1R12A (MYPT1), RPS6, or SLC9A1 (NHE1) [21,30–35].

Direct and indirect phosphorylation by ERK and RSK

Of the potential RSK substrates, discussed above, only 28 were PDZ-containing proteins, about half of which were identified only in a single data set (Fig. 5B). Only four direct RSK1 binders were identified in both the RSK compendium and in our holdup assay: ARHGEF11 and 12, MAST2, and SHROOM2. Notably, ARHGEF12 was identified in all phosphoproteo-

mic data sets as a PDZ-containing RSK substrate and was also the strongest binder of the unphosphorylated RSK1 peptide in the holdup assay. In addition, we have also found three additional partners (GRIP, SCRIB, NHERF1) binding to other RSK isoforms [18,5,25]. Conversely, it is worth noting that many of the strong RSK1 PBM binders (like GRID2IP, GOPC, PDZD7, or PDZRN4) do not contain any phosphorylation site matching the RSK1 consensus motif [16].

The RSK and the ERK compendiums show an overlap, indicating that some substrates can be phosphorylated by both RSK and ERK (Fig. 5AB). Although the MAPK- and the PBMs are found in the same C-terminal tail region of RSK where they are only separated by a few residues, it is stereochemically possible to form a ternary complex between the three domains [15]. Therefore, ERK can also phosphorylate RSK-bound PDZ proteins. We have found 8 RSK1 interaction partners that can be phosphorylated by ERK. One of them is ARHGEF12, which contains three RSK phosphorylation sites and a single MAPK phospho-site (Fig. 5C). In these cases, the C-terminal tail of RSK appears to serve a scaffolding role, bringing ERK and PDZ substrates close to each other.

To identify additional indirect, PDZ scaffold-mediated substrates, all potential interaction partners of our RSK1-binding PDZ scaffolds were collected from the IntAct PPI database [36]. This analysis revealed the significant enrichment of RSK and ERK substrates in many cases. For example, an interesting scaffold was MAGI1, which was not identified previously as a direct substrate of RSK (or ERK). MAGI1 has 74 potential interaction partners in that database; among which, more than 40% turn out to be potential RSK substrates. Similarly, 30% of MAGI1 potential interaction partners are potential ERK substrates, and 18% of them are potential substrates of both RSK and ERK (Fig. 5D, Table S3). We have found similarly significant enrichment of RSK/ERK substrates among various interaction partners, such as ARHGEF11. In conclusion, while only a small portion of RSK1-binding PDZ proteins may be direct substrates of RSK1, it appears that many of them may act as scaffolds, since many relevant potential RSK and ERK substrates can be found among their interaction partners.

Kinetic control of substrate phosphorylation

Next, we measured the kinetic parameters of PDZ–PBM interactions (Fig. S4). PDZ-bound fluorescent peptides were rapidly mixed with high molar excess of unlabeled peptides and changes in FP were monitored. Although the fluorescein label may alter the steady-state affinity of some interactions (Table 1), it probably affects only the dissociation rates, as usually observed for large hydrophobic groups. Under this assumption, unbiased off-rates for unlabeled peptides can be estimated (Fig. 6A). Our results revealed that

OFF dimmers have a generally slow binding kinetics (average $k_{off} \approx 210$ s^{-1}), while ON dimmers showed faster dissociation rates (average $k_{off} \approx 1100$ s^{-1}) (Fig. 6B). We used an *in silico* network-based modeling software to estimate substrate phosphorylation efficiency using these obtained kinetic parameters (Fig. S5) [37]. By using this simulation, the phosphorylated substrate levels, induced by the same amount of external stimulation, could be calculated and compared for ON and OFF switches (Fig. 6C). The analysis demonstrated that the presumed weaker interaction between OFF-dimmer PDZ domains and the active kinase should be compensated by a slower dissociation rate, thereby allowing for higher substrate phosphorylation.

Role of the RSK1 PBM in RhoA activation

RSK proteins have been proposed to play an important role in regulating cell motility, particularly through affecting the activity of the small GTPase protein, RhoA [38,21]. To this end, we have examined
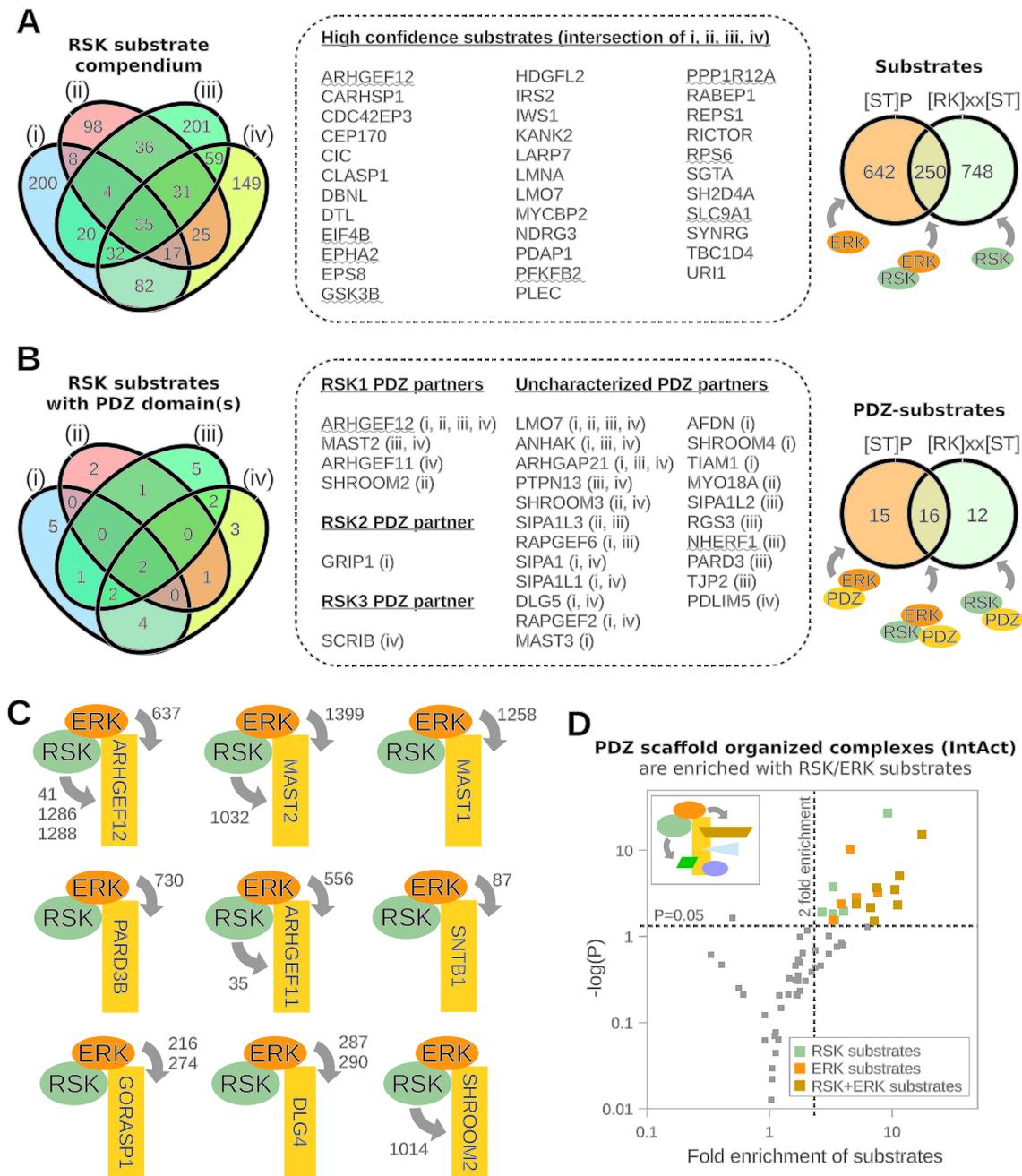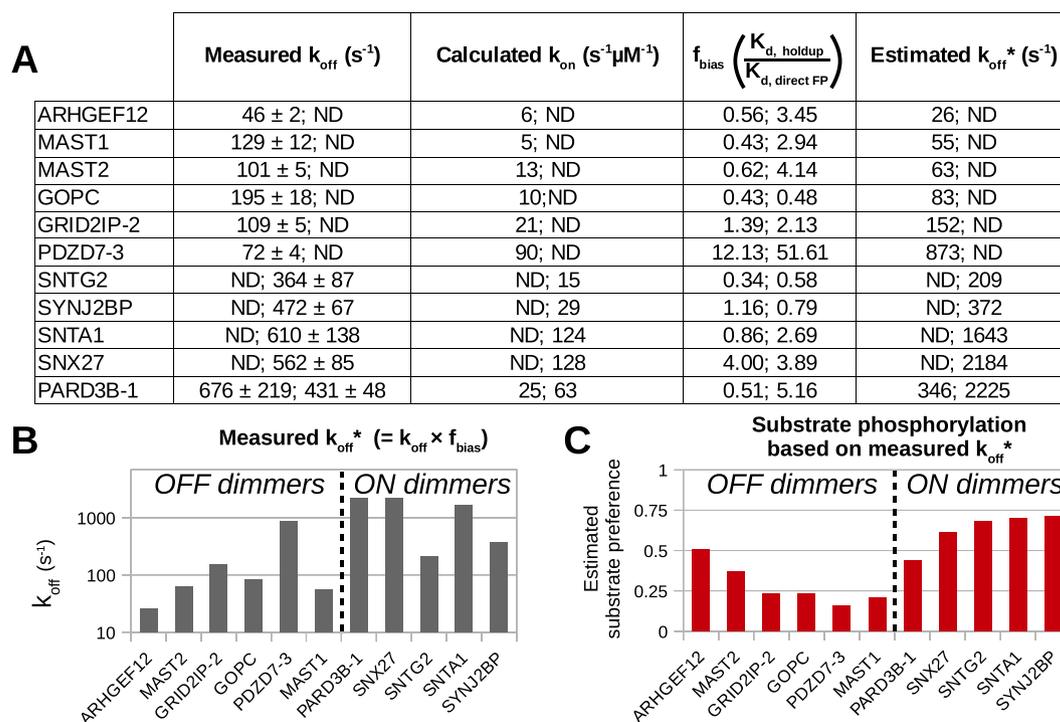

Fig. 5 (*legend on next page*)

A

	Measured k_{off} (s^{-1})	Calculated k_{on} (s^{-1}µM^{-1})	f_{bias} $\left(\dfrac{K_{d,\,holdup}}{K_{d,\,direct\ FP}}\right)$	Estimated k_{off}* (s^{-1})
ARHGEF12	46 ± 2; ND	6; ND	0.56; 3.45	26; ND
MAST1	129 ± 12; ND	5; ND	0.43; 2.94	55; ND
MAST2	101 ± 5; ND	13; ND	0.62; 4.14	63; ND
GOPC	195 ± 18; ND	10; ND	0.43; 0.48	83; ND
GRID2IP-2	109 ± 5; ND	21; ND	1.39; 2.13	152; ND
PDZD7-3	72 ± 4; ND	90; ND	12.13; 51.61	873; ND
SNTG2	ND; 364 ± 87	ND; 15	0.34; 0.58	ND; 209
SYNJ2BP	ND; 472 ± 67	ND; 29	1.16; 0.79	ND; 372
SNTA1	ND; 610 ± 138	ND; 124	0.86; 2.69	ND; 1643
SNX27	ND; 562 ± 85	ND; 128	4.00; 3.89	ND; 2184
PARD3B-1	676 ± 219; 431 ± 48	25; 63	0.51; 5.16	346; 2225

B   Measured k_{off}* (= k_{off} × f_{bias})

C   Substrate phosphorylation based on measured k_{off}*

Fig. 6. Binding kinetics differ between ON and OFF dimmers. (A) Dissociation rates were deduced from stopped flow FP experiments. On-rates are calculated based on the steady-state affinities of the fluorescent peptides (deduced from direct FP measurements). The bias factor (the ratio of the binding affinities of the direct FP and the holdup assay) was applied as a correction factor to the fitted dissociation rates to estimate unbiased off-rates. Values after the semicolon correspond to the phosphorylated RSK1 peptides. ND means not determined. (B) The corrected dissociation rates (k_{off}*) of a set of RSK1–PDZ interactions. Partners with OFF dimmer behavior showed a slower binding kinetics while ON dimmers preferred faster binding rates. (C) Substrate phosphorylation was calculated using an *in silico* model with measured dissociation rates.

the role of the RSK1 C-terminal region in RhoA activation. We transiently transfected a RSK1/2 knock-out HEK293T cell line with either full-length RSK1 (WT, 1–735) or a RSK1 construct with its C-terminal residue truncated (ΔC1, 1–734). We have found that over-expressed and phosphorylated RSK1 localized in the cytoplasm, similarly to the endogenous phospho-RSK in WT HEK293T cells (Fig. 7A) [15]. Interestingly, an increased level of basal RhoA activity was only apparent in the presence of the WT RSK1 construct (Fig. 7B). This slight increase was more pronounced in cells that were stimulated by the addition of serum.

Fig. 5. Meta-analysis of phosphoproteomic studies and bioinformatic search to find potential direct and indirect PDZ-dependent substrates of RSK and of ERK. (A) Left panel: a graphical representation of the intersections of RSK substrate lists from four different HTP phosphoproteomic studies: (i) Galan *et al.* [26], (ii) Moritz *et al.* [27], (iii) Avey *et al.* [28], and (iv) [RK]xx[ST] subset of the ERK compendium [29]. Middle panel: the intersection of the four lists contains several previously characterized RSK substrates (underlined), suggesting that other proteins found in this group may also represent high-confidence RSK substrates. Right panel: the RSK compendium and the direct ERK compendium greatly overlap, suggesting that a set of substrates can be phosphorylated on both ERK ([ST]P) and RSK ([RK]xx[ST]) consensus sites. (B) Same representation as in panel A but focusing on RSK substrates with PDZ domains. Only a few PDZ domain-containing substrates are present in the whole data set, and only a handful of them were found in more than one HTP study. Moreover, only four RSK1 binding partners were identified, from which only ARHGEF12 was found in the common group of the HTP studies. Uncharacterized PDZ partners may be direct partners of other RSK isoforms, or may be PDZ-independent substrates or false positives. (C) Many RSK1 PDZ interaction partners contain an ERK phosphorylation site. In addition, a few substrates, such as ARHGEF12, can be phosphorylated by both kinases. (D) The IntAct database was used to estimate the enrichment of ERK and RSK substrates among the interaction partners of the RSK1 PDZ-dependent interaction partners. On the vulcano plot, each dot represents the enrichment of kinase substrates among the interaction partners of a PDZ scaffold. We have identified a high number of potential indirect RSK and ERK substrates among these interaction partners, which are indicated with colors in the upper right corner. *P* values indicate statistical significance compared to a random pool of intracellular proteins, calculated by chi-square test. Fold enrichment indicates the increased proportions of substrates compared to the same random pool.
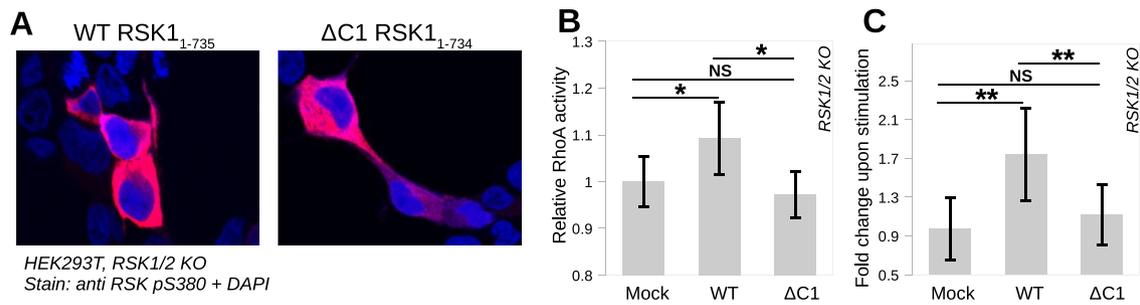
Fig. 7. The PBM of RSK1 links ERK activation to RhoA. (A) A RSK1/2 knockout HEK293T cell line was used to measure the role of the PBM of RSK1 in a native environment. Deletion of the RSK1 PBM does not affect the localization of active RSK1. (B) The presence of intact RSK1 increases the basal RhoA activity, but this effect is decreased without a functional PBM (n = 4). (C) Transfected and serum-starved cells were stimulated with serum (20% for 5 min). Without intact RSK1 (in the mock transfected knockout cell or in the presence of the PBM-lacking RSK1 construct), only minor increment was observed in the RhoA activity. The presence of intact, WT RSK1 enabled a proper response in RhoA activation upon stimulation (n = 4). Asterisks indicate statistical significance (**$P < 0.005$, *$P < 0.01$, NS $P > 0.01$) calculated by two-tailed Student's *t* test.

Stimulation increased RhoA activity in the presence of the WT RSK1 construct, but not in the presence of RSK ΔC1 (Fig. 7C). These results are consistent with a model postulating that the PBM of RSK1 serves as a docking motif for RSK1 to phosphorylate an important regulatory site in ARHGEF12, which then affects RhoA activation (Fig. S6) [39,40].

Discussion

Regulation of RSK1–PDZ interactions by PBM autophosphorylation

Previously, only a handful of PDZ interaction partners of RSK1 had been identified and their response to RSK1 autophosphorylation was largely unknown. Here, we characterized the PDZ interactome of RSK1 and examined how this changes upon PBM autophosphorylation at Ser732. Altogether, 34 interaction partners were identified with the holdup assay, most of them being novel, with the notable exception of MAGI1. In contrast to previous reports, we did not detect any interaction of RSK1 PBM with the first PDZ domain of NHERF (EBP50) and only detected a very weak affinity toward the first PDZ domain of Scribble (BI ≈ 0.17–0.18, corresponding to a dissociation constant of 60–70 μM) [25,18]. We do not think that this may be due to a lack of activity of these two domains in our assay, since both of them have already been positive with other PBMs in other holdup experiments. In particular, Scribble is positive with HPV16 E6 (BI ≈ 0.70, corresponding to a dissociation constant of 5–10 μM) [19]. Although most of the identified interactions were altered by PBM phosphorylation to some degree, we have found only a few cases that can be considered a genuine "phospho-switch." For example, detectable binding of RSK1 to ARHGEF12 and GRID2IP was mostly eliminated,

while binding to the adapter protein SNX27 was promoted by phosphorylation. In contrast, most substrates showed a "phospho-dimmer" effect, where phosphorylation *modulated* binding rather than *switching* it ON or OFF. Approximately as much ON as OFF dimmers were identified. These partners are able to interact with both states of the RSK1 PBM, albeit with different affinities. The rest of the interaction partners (such as PARD3B) displayed comparable affinities to both states of the RSK1 PBM, and therefore, these interaction partners are likely unable to sense the presence or absence of the phosphoryl group. Similar dimming mechanism was described on phosphorylation of PDZ domains themselves [41].

Mitogenic stimulation, such as that mediated by EGF, activates the MAPK pathway. Eventually, the downstream signals will activate ERK, leading to RSK1 phosphorylation and subsequent autophosphorylation in Ser732 of its PBM. Therefore, upon stimulation, we can expect dynamic changes in the RSK PBM-PDZ interactome based on quantitative *in vitro* measurements. To test this assumption, we created five intracellular PPI sensors for selected PDZ-dependent RSK1 interactions. In our assays, ARHGEF12, GOPC, and MAGI1 showed a preference for the native PBM, while the PDZ domain of SYNJ2BP preferred the phosphorylated PBM. In contrast, PARD3B could interact with both versions of RSK1. This cell-based protein–protein interaction study showed that EGF stimulation induces a phosphorylation-mediated rewiring of the RSK1–PDZ interactome inside cells, following the trends of the *in vitro* observations.

Further analysis on RSK and its PDZ-containing binding partners indicated that some of the latter are phosphorylated by RSK. Among the unambiguously identified RSK substrates, ARHGEF12 has a prominent place. It is a strong partner of the RSK1 peptide and their interaction is responsive to EGF stimulation. Moreover, Shi *et al.* [21] have recently showed that the

association between RSK2 and ARHGEF12 (also known as leukemia-associated RhoGEF or LARG) is essential in RhoA activation in glioblastoma cells. They discovered that RSK can interact with ARHGEF12 and phosphorylate it at Ser1288. They demonstrated that the presence of RSK is essential for the association between RhoA and ARHGEF12, and for subsequent RhoA activation. Inactivation or inhibition of RSK eliminated RhoA activation in response to extracellular stimulation. Our experiments gave similar results with RSK1, highlighting the central role of the RSK PBM in this process (Figs. 7 and S6).

Kinetic compensation in dynamic networks

Many direct substrates or substrate-tethering scaffolds of RSK (e.g., ARHGEF12 or MAGI1) contain an OFF dimmer PDZ domain. This creates a paradoxical situation, because the active kinase will down-regulate complex formation, and thus, only a smaller fraction of the kinase should be capable of mediating the phosphoryl transfer. Despite this, phosphorylation of such OFF dimmer type substrates can be detected with high confidence (e.g., Ser1288 of ARHGEF12). Here, we propose that the lifetime of these OFF dimmer interactions can substantially increase their phosphorylation. In our experiments, OFF dimmer PDZ domains showed 5 times slower dissociation rates than ON dimmer interactions (Figs. 6 and S4). This kinetic compensation can largely contribute to substrate phosphorylation (Fig. S5). We should emphasize here that these are general principles and they should be true for many other feedback-coupled enzymatic processes [42].

Phosphorylation-sensitive PDZ domains

Phosphorylation of PBMs is a very common regulatory mechanism in human cells [18]. Based on our experiments, we identified a set of PDZ domains that are responsible for mediating the OFF or ON dimmer effects of the phosphorylatable −3 position of the RSK PBM. Comparison of PDZ sequences reveals that there is no obvious driving force behind OFF dimmer behavior, but there are at least three positions within the peptide binding groove that can be important for ON dimmers (Fig. 8). The first of them is the outward facing residue of the second strand (βB) of the PDZ domain. This side chain is positioned in close proximity of the phosphate group, and while it is usually a Ser/Thr residue in PDZ domains, an Asn residue is preferred within ON dimmers. The other two altered side chains are within the third strand (βC) of the PDZ domain. Here, both external side chains are altered in ON dimmers. Interestingly, the closest residue to the phosphosite is most frequently a Ser residue and the other one is a basic amino acid. The role of two of these residues in the coordination of the phosphate group was captured in a crystal structure of SNX27 [43].
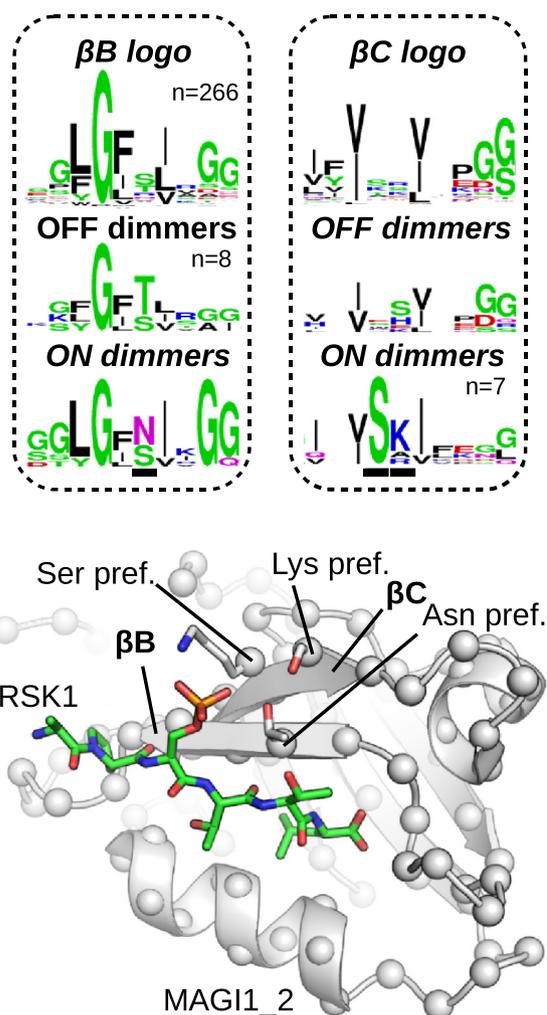

Fig. 8. Determinants of −3 phospho-PBM specificity. The PBM-binding groove of ON dimmer PDZ domains displays some notable sequence preferences. Sequence logos were generated from every human PDZ sequences or from identified dimmer subsets of the RSK1 peptide partners. Important differences are underlined in the ON dimmer sequence logo, and their side-chains are shown with sticks in the structure of the OFF dimmer MAGI1. In contrast to ON dimmers, no preferences was identified for OFF dimmers.

Asn56 from βB and Ser82 from βC mediate a hydrogen bond with the phosphate group of PBMs. Moreover, replacing the basic residue in the βC (Arg762) to Ala in Scribble can swap the RSK3 binding properties from ON- to OFF-dimmer [18]. These observations led us to the conclusion that ON dimmer propensity is determined by the presence of phosphate acceptor sites while OFF dimmer propensity is currently not understood. Further studies are needed to collect more evidence about such effects and classify PDZ domains on the basis of their response to phosphorylation events at different positions of their target PBM sequences.

Response to phosphorylation: switches and dimmers

Phosphorylation can alter linear motif binding by multiple ways. In the literature, most examples of phosphorylation-induced PPI changes are considered as switches (usually called "phospho- switches"), which can turn PPIs on or off. However, signaling processes are not solely based on binary events and may also involve fine-tuning mechanisms. A "switch" refers to binary transitions between two distinct states (the interaction occurs or does not occur), while a "dimmer" allows a fine tuning mechanism (smaller or larger changes in the affinity of an interaction). The dimming mechanism makes sense for describing events based on non-covalent interactions, however in some cases (e.g., in the context of additional binding events) synergism can enhance this effect resulting in switch-like changes. Our results demonstrate a continuum between ON and OFF switches, including many gradually altered dimmers, suggesting that, among phosphorylation-induced changes, ON/OFF dimmer effects may predominate, while ON/OFF switches represent only extreme cases.

Materials and Methods

Holdup assay

The automated holdup assay was carried out against peptides (RSK1$_{725-735}$) in triplicates as previously described [19] with minor modifications. In brief, we measured the fraction of PDZ depletion (BI) in the fluid phase during a pull-down experiment. For the detailed protocol, please look at Ref. [20]. The sequences of the clones of the PDZome v2 were designed according to [2]. All genes were codon optimized for *Escherichia coli* expression and cloned into a pETG41A plasmid. All protein constructs were expressed in *E. coli* following the previous protocol [19] with minimal modifications. All constructs were checked for solubility, and cell lysate soluble fractions were adjusted to approximately 4 μM concentration and frozen in 96-well plates. In addition, mass spectrometry was used to confirm the identity of each PDZ clones. For the detailed protocols of production and quality control, please look at Ref. [20]. We measured interactions against 255 proteins with the unphosphorylated peptide and against 252 proteins with the phosphorylated peptide. The missing proteins from the human PDZome (consisting of 266 proteins) showed problems with the expressions or stability of these constructs, or we had technical issues during the assay. In this work, BI = 0.2 was used as the minimal BI threshold value to define high-confidence PDZ–PBM pairs, as proposed previously [19]. Figure S1 contains the BI values of the RSK1 and phospho-RSK1 data sets. Data were analyzed as formerly

described [19]. All plots and calculations in this work were done using these conventional data sets. In addition, we already provide the values calculated with an updated protocol in the supplemental file, because the new calculation approach will set the standard for future holdup papers. These were generated using an automated computational protocol awaiting for publication. This updated analysis revealed three new interaction partners of the native RSK1 peptide (SCRIB-3, MPDZ-10, and RHPN1) and four new partners of the phosphorylated peptide (SCRIB-3, LIN7A, PDZRN3–2, and DLG3). Apart from these weak interaction partners, most values are coherent between calculations.

Protein expression and purification and peptide synthesis

Tandem affinity (Ni- and MBP-) purified MBP-PDZ proteins were used in biochemical assays. Unphosphorylated RSK1$_{683-735}$ peptides were recombinantly expressed with an N-terminal cleavable GST tag. After affinity purification, the GST tag was removed and the peptide was isolated by reverse phase HPLC. A fraction of the isolated peptide was phosphorylated with a constitutively active (T573E mutant) RSK1 C-terminal kinase domain as formerly described [19]. Unphosphorylated, phosphorylated, and fluorescein-labeled or -unlabeled RSK1$_{729-735}$ peptides were all chemically synthesized on an automated PSE Peptide Synthesizer (Protein Technologies, Tucson, AZ, USA) with Fmoc strategy. Biotinylated RSK1$_{725-735}$ peptides were purchased from JPT Innovative Peptide Solutions with 70%–80% purity. The biotin group was attached to the N-terminal *via* a TTDS linker. Protein (and Tyr containing peptide) concentrations were determined by UV spectroscopy. For peptides that lacked an aromatic residue, their dry mass was directly measured. Predicted peptide masses were confirmed by mass spectrometry.

Isothermal titration calorimetry

ITC measurements were carried out in 20 mM Hepes (pH 7.5), 150 mM NaCl, and 500 μM TCEP using a VP-ITC apparatus (MicroCal). MBP-PDZ domain (50 μM) was titrated with concentrated peptides at 37 °C. The Origin for ITC 5.0 (Originlab) software package was used for data processing.

Surface plasmon resonance

SPR measurements were performed on a Biacore T200 instrument equipped with CM5 sensor chip. Streptavidin was immobilized on the sensor chip with EDC-MS using a standard protocol. Biotinylated peptides (RSK1, pRSK1, HPV16E6) were immobilized on streptavidin, and after an extensive washing step, MBP-PDZ domains were injected onto the chip at eight

different concentrations and with two additional repli-cates. Unfortunately, our SPR analysis did not reveal the kinetic parameters of the studied PDZ–peptide interactions due to biphasic and very fast behavior. The saturated phase of the reference channel subtracted data was fitted with a hyperbolic function.

Steady-state FP

FP was measured in 384-well plates (Corning) using Synergy H4 multi-mode reader (BioTek). For direct titration experiments, 50 nM reporter peptide (RSK1$_{729–735}$) was mixed with increasing amount of MBP-PDZ domains. In competitive measurements, the 50 nM reporter peptide was mixed with the PDZ domain in a concentration to achieve high degree of complex formation. Subsequently, increasing amount of unlabeled peptide (RSK1$_{683–735}$) was added to the reaction mixture. Titration experiments were carried out in triplicate, and the average FP signal was used for fitting the data to a quadratic or competitive binding equation.

Monte Carlo modeling

To estimate the dissociation constant of weak interactions, we used the measured BI values from the HU assay. This parameter equals the bound fraction of the PDZ domain; therefore, it can be inserted directly into the general binding equation:

$$K_d = \frac{[PDZ_{free}] * [RSK_{free}]}{[PDZ–RSKcomplex]}$$
$$= \frac{([PDZ_{tot}] - BI * [PDZ_{tot}]) * ([RSK_{tot}] - BI * [PDZ_{tot}])}{BI * [PDZ_{tot}]}$$

Assuming that the total PDZ domain concentration is ~4 μM, the only unknown parameter is the total peptide concentration. Instead of a simple nonlinear fit, we have used an in-house Python script for Monte Carlo modeling and least squares fitting to utilize the standard deviations of the HU assay and the K_d measurements. Each fitting was repeated 10,000 times, and the average peptide concentration along with the lower and upper quartiles was plotted in Fig. 2B. Based on our SPR measurements, the RSK peptide concentra-tion should be around 20 μM (most probably between 18 and 21 μM). Direct FP indicates that this concen-tration should be around 14 μM (most probably between 6 and 20 μM). In the case of the competitive FP, we have found that the peptide concentration should be around 14 μM (most probably between 9 and 18 μM). For K_d extrapolation, we have used a peptide concentration of 17 μM.

Protein–protein interaction assay

The NanoBiT PPI MCS starter system was pur-chased from Promega. The N-terminus of RSK1 was tagged with the short NanoBiT tag (SmBiT) and either the N- or the C-terminus of the interaction partner with the large NanoBiT tag (LgBiT). Full-length RSK1 was cloned into pBit2.1-N[TK/SmBiT] vector. Full-length MAGI1 and ERK2 constructs were previously cloned into the LgBiT vector. Full-length ARHGEF12 (isoform 2), GOPC (isoform 2), PARD3B (1–913), and SYNJ2BP were cloned into the pBit1.1-N[TK/LgBiT] vectors. All constructs were cloned from HEK293T or HeLa cDNA pools and were confirmed by sequencing. HEK293T cells were cultured in Dulbecco's modified Eagle medium (Lonza) containing 10% fetal bovine serum and 1% penicillin/streptomycin/amphotericin B. 2×10^4 cells/well were seeded onto a white, TC-treated 96-well plate (Greiner) 24 h prior to transfection. Transient transfections were carried out with FuGene HD reagent (Promega) according to the NanoBiT system's instructions. Four hours after transfection, cells were starved for 20 h in CO_2-independent medium (Thermo). Cells were assayed 24 h after transfection using Nano-Glo reagent (Promega) and a Synergy H4 plate reader (BioTek). Experiments were carried out according to the manufacturer's instructions. To validate the interaction sensors, we compared the steady-state luminescence signals of different mutants in serum-starved cells. Stimulation was performed using 20 ng/ml EGF (Sigma-Aldrich). Each experiment was performed with at least six biological replicates. We must note that we observed that the observed periodicity in the luminescence appeared environment dependent, as even under slightly modified conditions (i.e., different media, cell density or protein expression level) no periodic features appeared.

Signaling pathway modeling

Rule-based network modeling was carried out with the software package BioNetGen with the ordinary differential equation solver running on a desktop PC. The simulated pathway was described in Fig. S5A. Pathway activation was initiated from a pre-equilibrated state. The simulation was initiated by introducing the "Stim" to the system. This simplified, artificial signal generator was adjusted to mimic the natural activation profile of the ERK pathway upon EGF stimulation.

Stopped-flow FP

Fast kinetic measurements were performed with the stopped-flow instrument SFM-300 (Bio-Logic) with polarized excitation at 488 nm. Parallel and perpen-dicular fluorescent emissions were measured through a 550 ± 20-nm band-pass filter (Comar Optics). All reactions were measured at 25 °C in a buffer containing 20 nM Hepes (pH 7.5), 150 mM NaCl, and 150 μM TCEP. Post-mixing fluorescent peptide concentration was 0.5 μM. The fluorescent peptide (RSK1$_{729–735}$) was pre-complexed with high amount of MBP-PDZ domain (5–40 μM, post-mix). To

measure the dissociation of the labeled peptide, we rapidly mixed the PDZ bound complex with high molar excess of unlabeled peptide (RSK1$_{729-735}$ 100 μM, post-mix). Each experiment was carried out multiple times (n > 9), and the averaged transients were fitted using a single exponential function. Corrections were applied to estimate the unbiased binding of an unlabeled peptide based on the dissociation constant differences between the direct FP measurements and the unbiased HU assay.

Immunofluorescence

For detection of the intracellular localization of transfected proteins, 1×10^5 cells/well were seeded onto a cover slip-containing (Assistent) 24-well plate. Cells were fixed with 4% PFA solution and blocked for 1 h in 5% BSA and 0.3% Triton-X 100, dissolved in PBS at room temperature. The RSK1/2 knockout (CRISPR) HEK293 cell line was a kind gift from Fanxiu Zhu. To introduce exogenous WT or mutant RSK1 into these cell lines, we created pIRES2-EGFP based vectors, which expressed untagged RSK1s along with a GFP transfection reporter gene. Phosphorylated RSK was detected with the help of anti-pRSK pSer380 (1:800, CST) primary and Alexa Fluor 647 (anti-rabbit, 1:800, Thermo) conjugated secondary antibodies. ARHGEF12 (isoform 2) was cloned into a pmCherry-C1 vector. Mutations were introduced by QuickChange site-directed mutagenesis. Nuclear staining was performed using DAPI (0.1 μg/ml). After washing, cover glasses were mounted to microscopy slides by Mowiol 4–88 mounting medium (Sigma-Aldrich). Confocal microscopy was carried out using a Zeiss LSM 710 system (Carl Zeiss Microscopy GmbH, Jena, Germany) with a 40× oil objective. Images were processed by the ImageJ software.

RhoA activation assay

The commercially available luminescence-based G-LISA RhoA activation assay (Cytoskeleton) was used to measure the GTP bound RhoA levels in cell cultures. 2×10^5 cells/well were seeded onto a 24-well plate. G-LISA assay was performed according to the manufacturer's recommendations, 24 h after transfection with the exception of the concentration and the antibody dilutions. Sample concentrations were equalized to 1 mg/ml. Primary and secondary antibodies were diluted to 1:500 and 1:1000, respectively. Luminescence signal was detected on a Synergy H4 plate reader (BioTek). The RSK inhibitor BI-D1870 treatment was performed at 100 nM for 1 h. The MEK inhibitor CI1040 was incubated ON at 100 nM. Inhibitor treatments were performed in Dulbecco's modified Eagle medium supplemented with 10% fetal bovine serum. Serum stimulation (20%) was performed with serum-starved cells for 5 min.

Supplementary data to this article can be found online at https://doi.org/10.1016/j.jmb.2019.01.038.

References

[1] V. Neduva, R.B. Russell, Linear motifs: evolutionary interaction switches, FEBS Lett. 579 (2005) 3342–3345, https://doi.org/10.1016/j.febslet.2005.04.005.

[2] K. Luck, S. Charbonnier, G. Travé, The emerging contribution of sequence context to the specificity of protein interactions mediated by PDZ domains, FEBS Lett. 586 (2012) 2648–2661, https://doi.org/10.1016/j.febslet.2012.03.056.

[3] M. Sheng, C. Sala, PDZ domains and the organization of supramolecular complexes, Annu. Rev. Neurosci. 24 (2001) 1–29, https://doi.org/10.1146/annurev.neuro.24.1.1.

[4] J. Saras, C.H. Heldin, PDZ domains bind carboxy-terminal sequences of target proteins, Trends Biochem. Sci. 21 (1996) 455–458, https://doi.org/10.1016/S0968-0004(96)30044-3.

[5] G.M. Thomas, G.R. Rumbaugh, D.B. Harrar, R.L. Huganir, Ribosomal S6 kinase 2 interacts with and phosphorylates PDZ domain-containing proteins and regulates AMPA receptor transmission, Proc. Natl. Acad. Sci. U. S. A. 102 (2005) 15006–15011, https://doi.org/10.1073/pnas.0507476102.

[6] F.J. Sulzmaier, S. Young-Robbins, P. Jiang, D. Geerts, A.M. Prechtl, M.L.M.L. Matter, S. Kesari, J.W. Ramos, RSK2 activity mediates glioblastoma invasiveness and is a potential target for new therapeutics, Oncotarget 7 (2016) 79869–79884, https://doi.org/10.18632/oncotarget.13084.

[7] K.G. Hartman, M.I. Vitolo, A.D. Pierce, J.M. Fox, P. Shapiro, S.S. Martin, P.T. Wilder, D.J. Weber, Complex formation between s100b protein and the p90 ribosomal S6 kinase (RSK) in malignant melanoma is calcium-dependent and inhibits extracellular signalregulated kinase (ERK)-mediated phosphorylation of RSK, J. Biol. Chem. 289 (2014) 12886–12895, https://doi.org/10.1074/jbc.M114.561613.

[8] J. Pouysségur, V. Volmat, P. Lenormand, Fidelity and spatio-temporal control in MAP kinase (ERKs) signalling, Biochem. Pharmacol. 64 (2002) 755–763, https://doi.org/10.1016/S0006-2952(02)01135-8.

[9] A. Alexa, G. Gógl, G. Glatz, Á. Garai, A. Zeke, J. Varga, E. Dudás, N. Jeszenői, A. Bodor, C. Hetényi, A. Reményi, Structural assembly of the signaling competent ERK2–RSK1 heterodimeric protein kinase complex, Proc. Natl. Acad. Sci. 112 (2015) 2711–2716, https://doi.org/10.1073/pnas.1417571112.

[10] M. Frödin, C.J. Jensen, K. Merienne, S. Gammeltoft, A phosphoserine-regulated docking site in the protein kinase RSK2 that recruits and activates PDK1, EMBO J. 19 (2000) 2924–2934, https://doi.org/10.1093/emboj/19.12.2924.

[11] M. Frödin, T.L. Antal, B.a. Dümmler, C.J. Jensen, M. Deak, S. Gammeltoft, R.M. Biondi, A phosphoserine/threonine-binding pocket in AGC kinases and PDK1 mediates activation by hydrophobic motif phosphorylation, EMBO J. 21 (2002) 5396–5407, https://doi.org/10.1093/emboj/cdf551.

[12] Á. Garai, A. Zeke, G. Gógl, I. Törő, F. Ferenc, H. Blankenburg, T. Bárkai, J. Varga, A. Alexa, D. Emig, M. Albrecht, A. Reményi, Specificity of linear motifs that bind to a common mitogen-activated protein kinase docking groove, Sci. Signal. 5 (2012), ra74. https://doi.org/10.1126/scisignal.2003004.Specificity.

[13] G. Gógl, A. Alexa, B. Kiss, G. Katona, M. Kovács, A. Bodor, A. Reményi, L. Nyitray, Structural basis of ribosomal S6 kinase 1 (RSK1) inhibition by S100B protein: modulation of the extracellular signal-regulated kinase (ERK) signaling cascade in a calcium-dependent way, J. Biol. Chem. 291 (2015) 11–27, https://doi.org/10.1074/jbc.M115.684928.

[14] S. Kang, S. Dong, A. Guo, H. Ruan, S. Lonial, H.J. Khoury, T. Gu, J. Chen, Epidermal growth factor stimulates RSK2 activation through activation of the MEK/ERK pathway and Src-dependent tyrosine phosphorylation of RSK2 at Tyr-529, 283 (2008) 4652–4657, https://doi.org/10.1074/jbc.M709673200.

[15] G. Gógl, B. Biri-Kovács, Á.L. Póti, H. Vadászi, B. Szeder, A. Bodor, G. Schlosser, A. Ács, L. Turiák, L. Buday, A. Alexa, L. Nyitray, A. Reményi, Dynamic control of RSK complexes by phosphoswitch-based regulation, FEBS J. 285 (2018) 46–71, https://doi.org/10.1111/febs.14311.

[16] P.V. Hornbeck, B. Zhang, B. Murray, J.M. Kornhauser, V. Latham, E. Skrzypek, PhosphoSitePlus, 2014: mutations, PTMs and recalibrations, Nucleic Acids Res. 43 (2015) D512–D520, https://doi.org/10.1093/nar/gku1267.

[17] K.N. Dalby, N. Morrice, F.B. Caudwell, J. Avruch, P. Cohen, Identification of regulatory phosphorylation sites in mitogen-activated protein kinase (MAPK)-activated protein kinase-1a/p90rsk that are inducible by MAPK, J. Biol. Chem. 273 (1998) 1496–1505, https://doi.org/10.1074/jbc.273.3.1496.

[18] G.N. Sundell, R. Arnold, M. Ali, P. Naksukpaiboon, J. Orts, P. Güntert, C.N. Chi, Y. Ivarsson, Proteome-wide analysis of phospho-regulated PDZ domain interactions, Mol. Syst. Biol. 14 (2018) 1–22, https://doi.org/10.15252/msb.20178129.

[19] R. Vincentelli, K. Luck, J. Poirson, J. Polanowska, J. Abdat, M. Blémont, J. Turchetto, F. Iv, K. Ricquier, M.-L. Straub, A. Forster, P. Cassonnet, J.-P. Borg, Y. Jacob, M. Masson, Y. Nominé, J. Reboul, N. Wolff, S. Charbonnier, G. Travé, Quantifying domain-ligand affinities and specificities by high-throughput holdup assay, Nat. Methods 12 (2015) 787–793, https://doi.org/10.1038/nmeth.3438.

[20] Y. Duhoo, V. Girault, J. Turchetto, L. Ramond, F. Durbesson, P. Fourquet, Y. Nominé, V. Cardoso, A.F. Sequeira, J.L.A. Brás, C.M.G.A. Fontes, G. Travé, N. Wolff, R. Vincentelli, High throughput production of a newly designed library of soluble human single and tandem PDZ domains allows semi-quantitative PDZ–peptide interaction screening through high throughput holdup assay., Methods Mol. Biol. in press (n.d.).

[21] G.-X. Shi, W.S. Yang, L. Jin, M.L. Matter, J.W. Ramos, RSK2 drives cell motility by serine phosphorylation of LARG and activation of Rho GTPases, Proc. Natl. Acad. Sci. 115 (2018) E190–E199, https://doi.org/10.1073/pnas.1708584115.

[22] L.R. Pearce, D. Komander, D.R. Alessi, The nuts and bolts of AGC protein kinases, Nat. Rev. Mol. Cell Biol. 11 (2010) 9–22, https://doi.org/10.1038/nrm2822.

[23] A.S. Dixon, M.K. Schwinn, M.P. Hall, K. Zimmerman, P. Otto, T.H. Lubben, B.L. Butler, B.F. Binkowski, T. MacHleidt, T.A. Kirkland, M.G. Wood, C.T. Eggers, L.P. Encell, K.V. Wood, NanoLuc complementation reporter optimized for accurate measurement of protein interactions in cells, ACS Chem. Biol. 11 (2016) 400–408, https://doi.org/10.1021/acschembio.5b00753.

[24] M. Cargnello, P.P. Roux, Activation and function of the MAPKs and their substrates, the MAPK-activated protein kinases, Microbiol. Mol. Biol. Rev. 75 (2011) 50–83, https://doi.org/10.1128/MMBR.00031-10.

[25] H.C. Lim, T.-S. Jou, Ras-activated RSK1 phosphorylates EBP50 to regulate its nuclear localization and promote cell proliferation, Oncotarget 7 (2016) 10283–10296, https://doi.org/10.18632/oncotarget.7184.

[26] J.A. Galan, K.M. Geraghty, G. Lavoie, E. Kanshin, J. Tcherkezian, V. Calabrese, G.R. Jeschke, B.E. Turk, B.A. Ballif, J. Blenis, P. Thibault, P.P. Roux, Phosphoproteomic analysis identifies the tumor suppressor PDCD4 as a RSK substrate negatively regulated by 14–3–3, Proc. Natl. Acad. Sci. 111 (2014) E2918–E2927, https://doi.org/10.1073/pnas.1405601111.

[27] A. Moritz, Y. Li, A. Guo, J. Villén, Y. Wang, J. MacNeill, J. Kornhauser, K. Sprott, J. Zhou, A. Possemato, J.M. Ren, P. Hornbeck, L.C. Cantley, S.P. Gygi, J. Rush, M.J. Comb, Akt–RSK–S6 kinase signaling networks activated by oncogenic receptor tyrosine kinases, Sci. Signal. 3 (2010) https://doi.org/10.1126/scisignal.2000998.

[28] D. Avey, S. Tepper, W. Li, Z. Turpin, F. Zhu, Phosphoproteomic analysis of KSHV-infected cells reveals roles of ORF45-activated RSK during lytic replication, PLoS Pathog. 11 (2015) 1–30, https://doi.org/10.1371/journal.ppat.1004993.

[29] E.B. Ünal, F. Uhlitz, N. Blüthgen, A compendium of ERK targets, FEBS Lett. 591 (2017) 2607–2615, https://doi.org/10.1002/1873-3468.12740.

[30] D. Shahbazian, P.P. Roux, V. Mieulet, M.S. Cohen, B. Raught, J. Taunton, J.W.B. Hershey, J. Blenis, M. Pende, N. Sonenberg, The mTOR/PI3K and MAPK pathways converge on eIF4B to control its phosphorylation and activity, EMBO J. 25 (2006) 2781–2791, https://doi.org/10.1038/sj.emboj.7601166.

[31] Y. Zhou, N. Yamada, T. Tanaka, T. Hori, S. Yokoyama, Y. Hayakawa, S. Yano, J. Fukuoka, K. Koizumi, I. Saiki, H. Sakurai, Crucial roles of RSK in cell motility by catalysing serine phosphorylation of EphA2, Nat. Commun. 6 (2015) 1–12, https://doi.org/10.1038/ncomms8679.

[32] R. Lara, M.J. Seckl, O.E. Pardo, The p90 RSK family members: common functions and isoform specificity, Cancer Res. 73 (2013) 5301–5308, https://doi.org/10.1158/0008-5472.CAN-12-4448.

[33] T. Houles, S.P. Gravel, G. Lavoie, S. Shin, M. Savall, A. Meant, B. Grondin, L. Gaboury, S.O. Yoon, J. St-Pierre, P.P. Roux, RSK regulates PFK-2 activity to promote metabolic rewiring in melanoma, Cancer Res. 78 (2018) 2191–2204, https://doi.org/10.1158/0008-5472.CAN-17-2215.

[34] M. Artamonov, K. Momotani, D. Utepbergenov, A. Franke, A. Khromov, Z.S. Derewenda, A.V. Somlyo, The p90 ribosomal S6 kinase (RSK) is a mediator of smooth muscle contractility, PLoS One 8 (2013), e58703. https://doi.org/10.1371/journal.pone.0058703.

[35] F. Cuello, A.K. Snabaitis, M.S. Cohen, J. Taunton, M. Avkiran, Evidence for direct regulation of myocardial Na+/H+ exchanger isoform 1 phosphorylation and activity by 90-kDa ribosomal S6 kinase (RSK): effects of the novel and specific RSK inhibitor fmk on responses to 1-adrenergic stimulation, Mol. Pharmacol. 71 (2006) 799–806, https://doi.org/10.1124/mol.106.029900.

[36] S. Kerrien, B. Aranda, L. Breuza, A. Bridge, F. Broackes-Carter, C. Chen, M. Duesbury, M. Dumousseau, M. Feuermann, U. Hinz, C. Jandrasits, R.C. Jimenez, J. Khadake, U. Mahadevan, P. Masson, I. Pedruzzi, E. Pfeiffenberger, P. Porras, A. Raghunath, B. Roechert, S. Orchard, H. Hermjakob, The IntAct molecular interaction database in 2012, Nucleic Acids Res. 40 (2012) 841–846, https://doi.org/10.1093/nar/gkr1088.

[37] L.A. Harris, J.S. Hogg, J.J. Tapia, J.A.P. Sekar, S. Gupta, I. Korsunsky, A. Arora, D. Barua, R.P. Sheehan, J.R. Faeder, BioNetGen 2.2: advances in rule-based modeling, Bioinformatics 32 (2016) 3366–3368, https://doi.org/10.1093/bioinformatics/btw469.

[38] M.D. Larrea, F. Hong, S.A. Wander, T.G. da Silva, D. Helfman, D. Lannigan, J.A. Smith, J.M. Slingerland, RSK1 drives p27Kip1 phosphorylation at T198 to promote RhoA inhibition and increase cell motility, Proc. Natl. Acad. Sci. 106 (2009) 9268–9273, https://doi.org/10.1073/pnas.0805057106.

[39] E. Grabocka, P.B. Wedegaertner, Disruption of oligomerization induces nucleocytoplasmic shuttling of leukemia-associated rho guanine-nucleotide exchange factor, Mol. Pharmacol. 72 (2007) 993–1002, https://doi.org/10.1124/mol.107.035162.

[40] R. Kristelly, G. Gao, J.J.G. Tesmer, Structural determinants of RhoA binding and nucleotide exchange in leukemia-associated rho guanine-nucleotide exchange factor, J. Biol. Chem. 279 (2004) 47352–47362, https://doi.org/10.1074/jbc.M406056200.

[41] S.W. Pedersen, L. Albertsen, G.E. Moran, B. Levesque, S.B. Pedersen, L. Bartels, H. Wapenaar, F. Ye, M. Zhang, M.E. Bowen, K. Strømgaard, Site-specific phosphorylation of PSD-95 PDZ domains reveals fine-tuned regulation of protein–protein interactions, ACS 12 (2017) 2313–2323, https://doi.org/10.1021/acschembio.7b00361.

[42] J. Corzo, M. Santamaria, Time, the forgotten dimension of ligand binding teaching, Biochem. Mol. Biol. Educ. 34 (2006) 413–416, https://doi.org/10.1002/bmb.2006.494034062678.

[43] T. Clairfeuille, C. Mas, A.S.M. Chan, Z. Yang, M. Tello-Lafoz, M. Chandra, J. Widagdo, M.C. Kerr, B. Paul, R.D. Teasdale, N.J. Pavlos, V. Anggono, B.M. Collins, A molecular code for endosomal recycling of phosphorylated cargos by the SNX27–retromer complex, Nat. Struct. Mol. Biol. 23 (2016) 921–932, https://doi.org/10.1038/nsmb.3290.